Inorg. Chem. **2007**, *46*, 6997–7004

Observation of a Mixed-Metal Transition in Heterobimetallic Au/Ag Dicyanide Systems

Samanthika R. Hettiarachchi,[†,||] Brian K. Schaefer,[†] Renante L. Yson,[†] Richard J. Staples,[‡] Regine Herbst-Irmer,[§] and Howard H. Patterson*[,†]

Department of Chemistry, University of Maine, Orono, Maine 04469, Department of Chemistry and Chemical Biology, Harvard University, 12 Oxford Street, Cambridge, Massachusetts 02138, and Department of Structural Chemistry, University of Göttingen, Tammannstrasse 4, D-37077 Göttingen, Germany

Received April 24, 2007

Crystals of the mixed-metal heterobimetallic Au/Ag dicyanide complex, $K[Au_xAg_{1-x}(CN)_2]$ ($x = 0 \rightarrow 1$), were obtained by slow evaporation. The mixed-metal complex $K[Au_{0.44}Ag_{0.56}(CN)_2]$ crystallizes in a rhombohedral crystal system, space group $R\bar{3}$. The crystal structure consists of layers of linear chains of $Au(CN)_2^-$ and $Ag(CN)_2^-$ ions and K^+ ions that connect the layers through the N atoms. The excitation and emission spectra of single crystals of $K[Au_xAg_{1-x}(CN)_2]$ were recorded at 4.2–180 K using excitation wavelengths between 230 and 260 nm. Two emission bands due to Ag–Au interactions were observed at 343 and 372 nm. Lifetime measurements indicate the shorter-wavelength emission corresponds to fluorescence and the longer-wavelength band is phosphorescence. These new emission bands are not seen in the pure $K[Ag(CN)_2]$ or pure $K[Au(CN)_2]$ crystals. Extended Hückel calculations show that the LUMO of the mixed-metal system is bonding while the HOMO is antibonding or very weakly bonding. Moreover, excited-state extended Hückel calculations indicate the formation of exciplexes with shorter metal–metal distances and higher metal–metal overlap populations than the corresponding ground-state oligomers. The luminescence is assigned to a mixed-metal transition from a molecular orbital with Au character to a molecular orbital with Ag character.

Introduction

A great deal of research has been focused on closed-shell d^{10} homometallic interactions in past decades largely due to their interesting photophysical properties.[1−8] These d^{10} closed-shell systems often have metal−metal distances which are less than the sum of the van der Waals radii of the elements.[9−12] This gives rise to a strong metallophilic interaction and is often cited as the origin of the luminescence observed in these complexes. Neutron diffraction,[13,14] X-ray crystallography,[15−23] luminescence,[16,18,24−26] Raman,[27−30] and

* To whom correspondence should be addressed. E-mail: howardp@maine.edu.
[†] University of Maine.
[||] Present address: Department of Chemistry, The Open University, Sri Lanka.
[‡] Harvard University.
[§] University of Göttingen.

(1) Pyykkö, P.; Runeberg, N.; Mendizabal, F. *Chem.−Eur. J.* **1997**, *3*, 1451−1457.
(2) Pyykkö, P.; Mendizabal, F. *Chem.−Eur. J.* **1997**, *3*, 1458−1465.
(3) Pyykkö, P.; Tamm, T. *Organometallics* **1998**, *17*, 4842−4852.
(4) Pyykkö, P.; Mendizabal, F. *Inorg. Chem.* **1998**, *37*, 3018−3025.
(5) Harvey, P. D.; Gray, H. B. *J. Am. Chem. Soc.* **1988**, *110*, 2145.
(6) Bardaji, M.; Laguna, A. *Eur. J. Inorg. Chem.* **2003**, 3069−3079.
(7) Shorrock, C. J.; Xue, B.-Y.; Kim, P. B.; Batchelor, R. J.; Patrick, B. O.; Leznoff, D. B. *Inorg. Chem.* **2002**, *41*, 6743−6753.
(8) Zhang, H.; Cai, J.; Feng, X.-L.; Li, T.; Li, X.-Y.; Ji, L.-N. *Inorg. Chem. Commun.* **2002**, *5*, 637−641.
(9) Schmidbaur, H.; Brachthauser, B.; Steigelmann, O. *Angew. Chem., Int. Ed. Engl.* **1991**, *30*, 1488−1490.
(10) Schmidbaur, H.; Weidenhiller, G.; Steigelmann, O. *Angew. Chem., Int. Ed. Engl.* **1991**, *30*, 433−435.
(11) Schmidbaur, H. *Gold Bull.* **2000**, *33*, 3−10.
(12) Schmidbaur, H.; Hamel, A.; Mitzel Norbert, W.; Schier, A.; Nogai, S. *Proc. Natl. Acad. Sci. U.S.A.* **2002**, *99*, 4916−21.
(13) Fischer, P.; Lucas, B.; Omary, M. A.; Larochelle, C. L.; Patterson, H. H. *J. Solid State Chem.* **2002**, *168*, 267−274.
(14) Fischer, P.; Lucas, B.; Patterson, H. H.; Larochelle, C. L. *Appl. Phys. A: Mater. Sci. Process.* **2002**, *74*, S1296−S1298.
(15) Leznoff, D. B.; Xue, B.-Y.; Patrick, B. O.; Sanchez, V.; Thompson, R. C. *Chem. Commun.* **2001**, 259−260.
(16) Burini, A.; Mohamed, A. A.; Fackler, J. P. *Comments Inorg. Chem.* **2003**, *24*, 253−280.
(17) Van Zyl, W. E.; Lopez-De-Luzuriaga, J. M.; Fackler, J. P., Jr.; Staples, R. J. *Can. J. Chem.* **2001**, *79*, 896−903.
(18) Fernandez, E. J.; Gimeno, M. C.; Laguna, A.; Lopez-de-Luzuriaga, J. M.; Monge, M.; Pyykkö, P.; Sundholm, D. *J. Am. Chem. Soc.* **2000**, *122*, 7287−7293.
(19) Copley, R. C. B.; Mingos, D. M. P. *J. Chem. Soc., Dalton Trans.* **1992**, 1755−1756.
(20) Teo, B. K.; Zhang, H. *Inorg. Chem.* **1991**, *30*, 3115−16.

10.1021/ic700780k CCC: $37.00
Published on Web 07/28/2007

UV−vis[19,26] spectroscopic techniques have been used to investigate these metal−metal interactions. Extended Hückel calculations along with ab initio methods have been employed to model their ground- and excited-state properties. Secondary interactions attributed to aurophilicity have been calculated to be 21−46 kJ/mol, which is on the order of the dissociation energy of a hydrogen bond. Larger clusters of Cu_n, Ag_n, and Au_n ($n = 5-8$) have been investigated through a variety of techniques and have been used as catalysts,[31−37] semiconductors, optical devices, pharmaceuticals, and antimicrobial agents.[38−41]

Two-coordinate gold complexes are usually colorless; however, they can be luminescent depending on the ligand and the extent of metal−metal interaction. For example, we have recently shown that dicyanoaurate(I) and dicyanoargentate(I) ions undergo significant oligomerization in aqueous and methanolic solutions.[26,42] We observed that the absorption edges of $K[Au(CN)_2]$ and $K[Ag(CN)_2]$ solutions undergo progressive red-shifts with an increase in concentration up to near the saturation limits. Two types of deviation from Beer's law were observed, a negative deviation for monomers' MLCT bands and a positive deviation for the oligomers' bands. Increasing the concentration within a given concentration range leads to red-shifts in the oligomers' absorption and/or excitation bands dominant in that range, while further increases in concentration lead to the appearance of new lower energy bands. These observations provide evidence for the formation of homometallic dimers and trimers in solution.

The crystal structure[43] and luminescent properties[44] of $K[Au(CN)_2]$ have been thoroughly investigated. It has been found that the nearest-neighbor distance between the gold atoms in the crystal structure varies as a function of cation. For example, in $K[Au(CN)_2]$ the gold atoms are separated by 3.64 Å, but when the cation is changed to tetrabutylammonium, the nearest-neighbor Au separation becomes 8.8 Å.[45] We have shown that the room-temperature emission spectrum of $K[Au(CN)_2]$ consists of a high-energy band at about 390 nm and a low-energy band at about 630 nm.[44] At 8 K, the high-energy band shows vibronic structure, while the low-energy band disappears. A comparison of the emission band energies with Au−Au separation indicates that the high-energy emission band should be assigned to states arising from Au−Au overlaps in two dimensions.

Compared to homometallic coordination compounds, few examples have been reported in the literature about heterometallic coordination compounds. Among these examples, Rawashde-Omary et al.[46] have reported about a new class of heterobimetallic compound, $AgAu(MTP)_2$ where MTP is diphenylmethylenethiophosphinate, which shows argento−aurophilic bonding interactions and a metal−metal distance of 2.912 Å. Also, Fernandez et al.[18,47] have reported DFT calculations with luminescent spectra for $[Au_2Ag_2(C_6F_5)_4(OCMe_2)_2]_n$ moieties showing a Au−Au distance of 3.16 Å and a Au−Ag distance of 2.79 and 2.78 Å. In these compounds, the emission profile observed in dilute acetone solution was assigned to ligand localized $\pi\pi^*$ excited states or to π-MMCT transitions, while the solid-state emission was assigned as arising from metal-centered $(d\sigma^*)^1(p\sigma)^1$ or $(d\delta^*)^1(p\sigma)^1$ excited states. Similar to our report on aqueous and methanolic solutions of $K[Au(CN)_2]$ and $K[Ag(CN)_2]$, the absorption and emission spectra of the compound in acetone display a band that does not obey the Lambert−Beer law. This deviation is consistent with the molecular aggregation in solution through gold−gold interactions. Very recently, Fackler et al. reported the synthesis and characterization of trinuclear mixed-metal silver and gold complexes containing carbeniate or imidazolate ligands.[48] These complexes exhibited short Au−Ag and Au−Au distances of ~3.3 and 3.2 Å, respectively.

Our group has recently reported the metallophilic interactions in closed-shell d^{10} metal−metal dicyanide-bonded systems $Eu[Ag_xAu_{1-x}(CN)_2]_3$ ($x = 0 \rightarrow 1$)[30] and $La[Ag_xAu_{1-x}(CN)_2]_3$ ($x = 0 \rightarrow 1$).[49,50] The presence of mixed-metal Au−

(21) Teo, B. K.; Shi, X.; Zhang, H. *J. Am. Chem. Soc.* **1991**, *113*, 4329−31.
(22) Teo, B. K.; Zhang, H.; Shi, X. *Inorg. Chem.* **1990**, *29*, 2083−91.
(23) Kanters, R. P. F.; Schlebos, P. P. J.; Bour, J. J.; Bosman, W. P.; Smits, J. M. M.; Beurskens, P. T.; Steggerda, J. J. *Inorg. Chem.* **1990**, *29*, 324−328.
(24) Assefa, Z.; DeStefano, F.; Garepapaghi, M. A.; LaCasce, J. H., Jr.; Ouellete, S.; Corson, M. R.; Nagle, J. K.; Patterson, H. H. *Inorg. Chem.* **1991**, *30*, 2868−2876.
(25) Markert, J. T.; Blom, N.; Roper, G.; Perregaux, A. D.; Nagasundaram, N.; Corson, M. R.; Ludi, A.; Nagle, J. K.; Patterson, H. H. *Chem. Phys. Lett.* **1985**, *118*, 258−62.
(26) Rawashdeh-Omary, M. A.; Omary, M. A.; Patterson, H. H.; Fackler, J. P., Jr. *J. Am. Chem. Soc.* **2001**, *123*, 11237−11247.
(27) Che, C.-M.; Lai, S.-W. *Coord. Chem. Rev.* **2005**, *249*, 1296−1309.
(28) Che, C.-M.; Tse, M.-C.; Chan, M. C. W.; Cheung, K.-K.; Phillips, D. L.; Leung, K.-H. *J. Am. Chem. Soc.* **2000**, *122*, 2464−2468.
(29) Cheng, E. C.; Leung, K. H.; Miskowski, V. M.; Yam, V. W.; Phillips, D. L. *Inorg. Chem.* **2000**, *39*, 3690−3695.
(30) Colis, J. C. F.; Staples, R.; Tripp, C.; Labrecque, D.; Patterson, H. H. *J. Phys. Chem. B* **2005**, *109*, 102−109.
(31) Li, D.; Che, C. M.; Kwong, H. L.; Yam, V. W. W. *J. Chem. Soc., Dalton Trans.* **1992**, 3325−9.
(32) Li, J. J.; Peng, X. *J. Nanosci. Nanotechnol.* **2004**, *4*, 565−568.
(33) Kanan, S. M.; Tripp, C. P.; Austin, R. N.; Patterson, H. H. *J. Phys. Chem. B* **2001**, *105*, 9441−9448.
(34) Kanan, S. M.; Kanan, M. C.; Patterson, H. H. *Curr. Opin. Solid State Mater. Sci.* **2003**, *7*, 443−449.
(35) Li, X. Z.; Li, F. B. *Environ. Sci. Technol.* **2001**, *35*, 2381−2387.
(36) Currao, A.; Reddy, V. R.; Calzaferri, G. *ChemPhysChem* **2004**, *5*, 720−724.
(37) Lopez, N.; Norskov, J. K. *J. Am. Chem. Soc.* **2002**, *124*, 11262−11263.
(38) Ni Dubhghaill, O. M.; Sadler, P. J. *Met. Complexes Cancer Chemother.* **1993**, 221−48.
(39) Shaw, C. F., III Gold complexes with antiarthritic, antitumour and anti-HIV activity. In *Uses of Inorganic Chemistry in Medicine*; Farrell, N. P., Ed.; Royal Society of Chemistry: Cambridge, 1999; pp 26−57.
(40) Gibson, C. S. *Chem. Prod. Chem. News* **1938**, *1*, 35−6.
(41) Tiekink, E. R. T. *Gold Bull.* **2003**, *36*, 117−124.
(42) Rawashdeh-Omary, M. A.; Omary, M. A.; Patterson, H. H. *J. Am. Chem. Soc.* **2000**, *122*, 10371−10380.
(43) Rosenzweig, A.; Cromer, D. T. *Acta Crystallogr.* **1959**, *12*, 709−12.
(44) Nagasundaram, N.; Roper, G.; Biscoe, J.; Chai, J. W.; Patterson, H. H.; Blom, N.; Ludi, A. *Inorg. Chem.* **1986**, *25*, 2947−51.
(45) Mason, W. *J. Am. Chem. Soc.* **1976**, *98*, 5182−5187.
(46) Rawashdeh-Omary, M. A.; Omary, M. A.; Fackler, J. P., Jr. *Inorg. Chim. Acta* **2002**, *334*, 376.
(47) Fernandez, E. J.; Lopez-de-Luzuriaga, J. M.; Monge, M.; Rodriguez, M. A.; Crespo, O.; Gimeno, M. C.; Laguna, A.; Jones, P. G. *Chem.−Eur. J.* **2000**, *6*, 636.
(48) Mohamed, A. A.; Galassi, R.; Papa, F.; Burini, A.; Fackler, J. P., Jr. *Inorg. Chem.* **2006**, *45*, 7770−7776.
(49) Colis, J. C. F.; Larochelle, C.; Fernandez, E. J.; Lopez-de-Luzuriaga, J. M.; Monge, M.; Laguna, A.; Tripp, C.; Patterson, H. H. *J. Phys. Chem. B* **2005**, *109*, 4317−4323.

Ag clusters in these species was verified using Raman and luminescence spectroscopy. These mixed-metal complexes exhibit many of the desirable properties of the pure dicyanoaurate and dicyanoargentate species including tunability for excited-state energy transfer. They luminesce quite strongly at room temperature at an energy that is tunable depending on the Au/Ag stoichiometric ratio, and the emission energy lies between those of the pure Au and Ag systems. This provides evidence that the excited states responsible for this emission are delocalized over the Ag and Au centers. The ability to tune the excited-state properties has far-reaching implications in the design of optical devices.

In this paper, we discuss the synthesis and characterization of $d^{10}-d^{10}$ heterometallic compounds containing gold and silver and compare the results with the corresponding pure systems. Whereas our previously reported Au/Ag systems contained +3 counterions, in the present article we study the luminescent properties of a Au/Ag system when the counterion is +1. Photoluminescence spectroscopy has been used as the major tool to study these systems. Here, we aim to synthesize and characterize mixed-metal gold−silver dicyanides and explain their interesting properties through a series of experiments.

Experimental Section

General Procedure and Physical Measurements. Reagent grade $K[Au(CN)_2]$ (Alfa-Aesar) and $K[Ag(CN)_2]$ (Alfa-Aesar) were used as received. For crystals of $K[Au_{0.44}Ag_{0.56}(CN)_2]$, a 4 mL aqueous solution of $K[Au(CN)_2]$ (0.861 mmol, 0.248 g) and 4 mL aqueous solution of $K[Ag(CN)_2]$ (0.860 mmol, 0.171 g) were mixed in a 25 mL beaker at room temperature. The resulting solution was covered with a watch glass, left undisturbed in a hood, and the solvent was allowed to evaporate slowly. After 4−5 days, colorless crystals were harvested. The mixture was expected to have a 0.50:0.50 (Ag/Au) mole ratio in the resulting crystal. However, after elemental and crystallographic analysis, it was found to have a 0.556(7):0.444(7) (Ag/Au) ratio (see X-ray Crystallography section below).

The other mixed-metal complexes were prepared in a similar manner by mixing the proper stoichiometric solutions (4 mL each) of $K[Au(CN)_2]$ and $K[Ag(CN)_2]$ in a 25 mL beaker. Crystals of $K[Au_xAg_{1-x}(CN)_2]$ ($x = 0 \rightarrow 1$) were harvested after 2−4 days.

The amount of Au and Ag present in the crystals was determined by atomic absorption spectroscopy using a Smith-Hieftje Model 857 atomic absorption spectrometer with flame ionizer. Standard solutions were prepared by serial dilutions from Puro-Graphic standard gold (998 μg/mL Au in 5% HCl) and silver (995 μg/mL Ag in 5% HCl) solutions purchased from Cole−Parmer Company. Steady-state photoluminescence spectra were recorded with a model QuantaMaster-1 fluorescence spectrophotometer from Photon Technology International (PTI). The instrument is equipped with two excitation monochromators and a 75 W xenon arc lamp. Luminescence spectra were recorded as a function of temperature using liquid helium as the coolant in a Model LT-3-110 Heli-Tran cryogenic liquid transfer system equipped with a temperature controller. Excitation spectra were corrected for variation of the lamp intensity using the Rhodamine B quantum counter. Emission spectra were uncorrected unless otherwise specified. Lifetime measurements were performed using a Nanophase diode-pumped solid-state laser that pulses at 266 nm with a repetition rate of 8.1 kHz. The decays were averaged over 1000 sweeps on the oscilloscope. All measurements were carried out for the same single crystals used in the elemental analysis, luminescence, and X-ray measurements.

X-ray Crystallographic Analysis. The crystal structure was determined using a Bruker SMART CCD-based diffractometer equipped with an LT-3 low-temperature apparatus operating at 213 K. A suitable crystal was chosen and mounted on a glass fiber using grease. Data were measured using ω scans of 0.3° per frame for 30 s, such that a hemisphere was collected. A total of 1271 frames were collected with a maximum resolution of 0.76 Å. The first 50 frames were recollected at the end of data collection to monitor for decay. Cell parameters were retrieved using SMART[51] software and refined using SAINT[52] software on all observed reflections. Data reduction was performed using the SAINT software which corrects for Lp and decay. Absorption corrections were applied using SADABS[53,54] supplied by George Sheldrick. The structure was solved by direct methods using the SHELXS-97 program[55] and refined by the least-squares method on F^2, SHELXL-97,[56] incorporated in SHELXTL-PC V 6.10.[57]

The structure was solved in the space group $R\bar{3}$ (No. 148) by analysis of systematic absences. The crystal was twinned with the twin law 0 −1 0 −1 0 0 0 0 −1. It was refined with the protocol described in Herbst-Irmer and Sheldrick.[58] The fractional contribution of the minor domain refined to 0.240(3). All atoms are refined anisotropically. The Au and Ag reside on the same site, and the occupancy was refined using the same coordinates and displacement parameters for both atoms. Refinement of the Ag/Au ratio gives values of 0.556(7):0.444(7) for the mixed-metal complex. The K^+ ion resides in two possible sites. The crystal used for the diffraction study showed no decomposition during data collection.

Computational Calculations. Extended Hückel[59] calculations were carried out for the ground and first excited states of the $[Au(CN)_2^-]_2$ dimer, $[Ag(CN)_2^-]_2$ dimer, and $[Au(CN)_2^-/Ag(CN)_2^-]$ dimer. Each unit of $[Au(CN)_2^-]$ and $[Ag(CN)_2^-]$ was assumed to have linear geometry. Bond distances for $K[Au(CN)_2]$ and $K[Ag(CN)_2]$ were taken from the X-ray crystallographic data, which are similar to those previously reported in the literature.[43] Potential energy diagrams of the ground and first excited states were generated by calculating the energy of each dimer as the metal−metal separation is varied. Calculations (extended Hückel and semiempirical methods) were also performed on pure and mixed-metal systems where a $Au(CN)_2^-$ or $Ag(CN)_2^-$ unit is surrounded by four other units in a rectangular arrangement (D_{2h}). This closely approximates the arrangement of the ions in the crystal. The program ICON-EDIT[60] was used in the extended Hückel calcula-

(50) Colis, J. C. F.; Larochelle, C.; Staples, R.; Herbst-Irmer, R.; Patterson, H. H. *Dalton Trans.* **2005**, 675−679.

(51) *SMART V 5.625 (NT) Software for the CCD Detector System*; Bruker Analytical X-ray Systems: Madison, WI, 2001.

(52) *SAINT V 6.22 (NT) Software for the CCD Detector System*; Bruker Analytical X-ray Systems: Madison, WI, 2001.

(53) Blessing, R. *Acta Crystallogr. A* **1995**, *51*, 33.

(54) Sheldrick, G. M. *SADABS-A Program for Empirical Absorption Correction*, Version 2006/1; University of Göttingen: Göttingen, Germany, 2006.

(55) Sheldrick, G. M. *SHELXS-90, Program for the Solution of Crystal Structure*; University of Göttingen: Göttingen, Germany, 1990.

(56) Sheldrick, G. M. *SHELXL-97, Program for the Refinement of Crystal Structure*; University of Göttingen: Göttingen, Germany, 1997.

(57) *SHELXTL 6.1 (PC-Version), Program library for Structure Solution and Molecular Graphics*; Bruker Analytical X-ray Systems: Madison, WI, 2000.

(58) Herbst-Irmer, R.; Sheldrick, G. M. *Acta Crystallogr. B* **2002**, *58*, 477−481.

(59) Hoffmann, R. *J. Chem. Phys.* **1963**, *39*, 1397.

Table 1. Crystallographic Data for $K[Au_{0.44}Ag_{0.56}(CN)_2]$[a]

empirical formula	$C_2Ag_{0.56}Au_{0.44}KN_2$
fw	238.61
space group	$R\bar{3}$
a (Å)	7.272(2)
c (Å)	26.563(3)
V (Å^3)	1216.5(5)
Z	9
D_{calcd} (Mg/m^3)	2.931
reflns collected	2881
data/restraints/params	653/0/33
R1[b] ($I > 2\sigma(I)$)/GOF	0.0193/1.079
wR2[c] ($I > 2\sigma(I)$)	0.0486

[a] Obtained with graphite-monochromated Mo Kα ($\lambda = 0.71073$ Å) radiation. [b] $R1 = \sum||F_o| - |F_c||/\sum|F_o|$. [c] $wR2 = \{\sum[w(F_o^2 - F_c^2)^2]/\{\sum[w(F_o^2)^2]\}\}^{1/2}$.

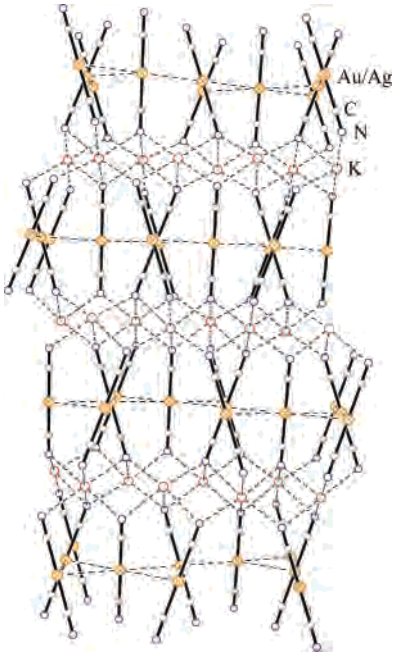

Figure 1. Layered structure of $K[Au_{0.44}Ag_{0.56}(CN)_2]$ with linear $M(CN)_2^-$ chains and K^+ ions connecting the layers through N contacts.

tions. Relativistic parameters for Au, Ag, C, and N were used as described elsewhere.[61,62]

Results and Discussion

X-ray Crystallography. Crystal data are summarized in Table 1. Figure 1 shows the crystal structure of the mixed-metal species $K[Au_{0.44}Ag_{0.56}(CN)_2]$. The Au and Ag atoms reside on the same site, and the occupancy was refined using the same coordinates and displacement parameters for both atoms. After refinement, a Ag/Au ratio of 56:44 was obtained. The C−Au−C and C−Ag−C bond angles are 180°. The crystal structure consists of layers of linear chains of $Au(CN)_2^-$ and $Ag(CN)_2^-$ and K^+ ions that connect the layers through N atoms. This is similar to the crystal structure of pure $K[Au(CN)_2]$ and $K[Ag(CN)_2]$ and the reported mixed-metal complexes $Eu[Au_xAg_{1-x}(CN)_2]_3$ and $La[Au_xAg_{1-x}(CN)_2]_3$ ($x = 0 \rightarrow 1$).[30,50] Table 2 shows the metal−metal distances in $K[Au_{0.44}Ag_{0.56}(CN)_2]$ in comparison to $K[Au(CN)_2]$ and $K[Ag(CN)_2]$.

Table 2. Metal−Metal Distances for $K[Au_{0.44}Ag_{0.56}(CN)_2]$, Pure $K[Au(CN)_2]$, and $K[Ag(CN)_2$

complex	M···M	distance, Å
$K[Au(CN)_2]$[a]	Au···Au	3.620(1)
$K[Au_{0.44}Ag_{0.56}(CN)_2]$ (HP30T)	Au···Au	3.636(1)
	Ag···Ag	3.636(1)
$K[Ag(CN)_2]$[a]	Ag···Ag	3.702(1)
	Ag···Ag	3.622(1)

[a] Unpublished results from our laboratories.

While many attempts were made to grow X-ray quality crystals, only one mixed-metal sample gave suitable data for X-ray structure determination. The Au/Ag stoichiometric ratio in the other mixed-metal samples were determined by atomic absorption spectroscopy. The luminescence spectra of these crystals do not differ markedly from the luminescence spectra of $K[Au_{0.44}Ag_{0.56}(CN)_2]$ for which a crystal structure was obtained.

Luminescence. Variable-temperature luminescence spectra for all crystals used in this study were recorded in the range of 180−4.2 K. New emissive states which are not present in the pure $K[Ag(CN)_2]$ or $K[Au(CN)_2]$ luminescence spectra are seen in the spectra of the mixed-metal $K[Au_xAg_{1-x}(CN)_2]$, with x between 0 and 1.

In Figure 2, the emission spectra for single crystals of $K[Au_xAg_{1-x}(CN)_2]$ at 4.2 K with $\lambda_{ex} = 265$ nm, and $x =$

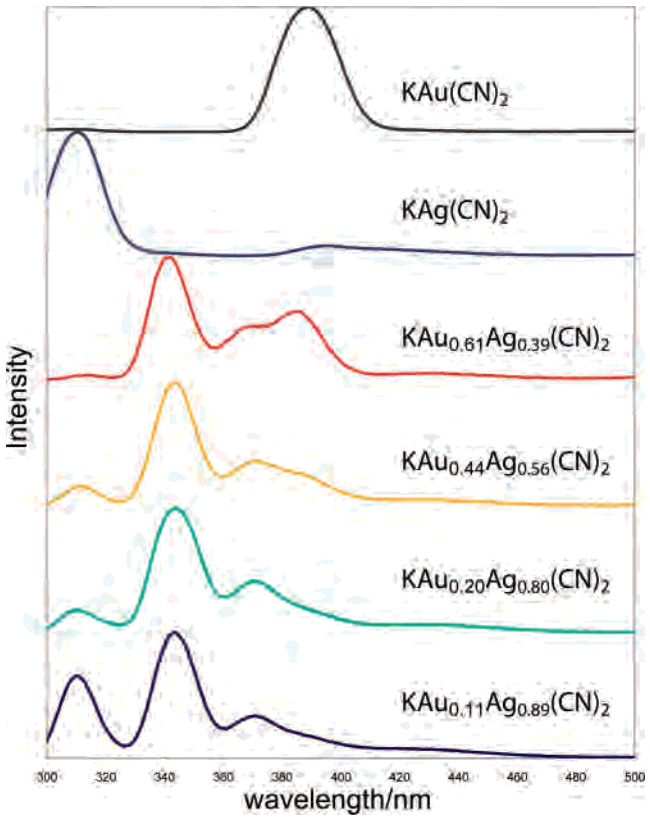

Figure 2. Emission spectra of $K[Au_xAg_{1-x}(CN)_2]$ ($x = 0 \rightarrow 1$) at 4.2 K with $\lambda_{ex} = 265$ nm as the metal composition is changed. Emission bands at 343 and 372 nm appear in the mixed-metal systems and not in the pure metal systems and are assigned to mixed-metal transitions.

(60) Calzaferri, G.; Rytz, R.; Braendle, M.; Bruehwiler, D.; Glaus, S. ICONEDiT: Extended Huckel molecular orbital and transition dipole moment calculations, update 2000. http://iacrs1.unibe.ch (August 26, 2006).
(61) Omary, M. A.; Patterson, H. H.; Shankle, G. *Mol. Cryst. Liq. Cryst. Sci. Technol., Sect. A* **1996**, *284*, 399−409.
(62) Pyykkö, P. *Chem. Rev.* **1988**, *88*, 563−94.

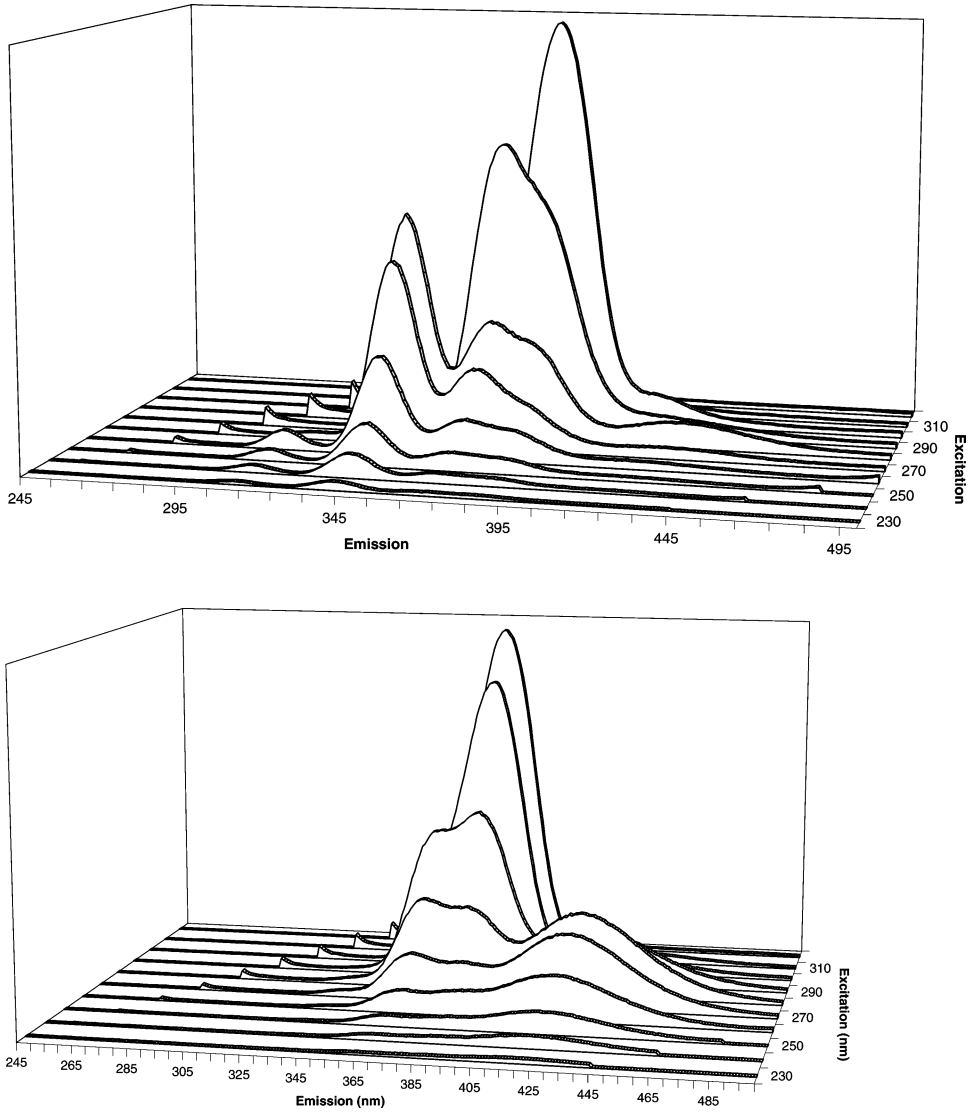

Figure 3. Three-dimensional emission of $K[Au_{0.61}Ag_{0.39}(CN)_2]$ showing the different fluorophores present at 4.2 (top) and 77 K (bottom) and their dependence on the excitation wavelength when the excitation wavelength is changed by 10 nm between each spectrum.

0→1 are shown. Pure $K[Au(CN)_2]$ shows a broad emission band at 386 nm, while pure $K[Ag(CN)_2]$ shows a broad band centered at 312 nm. The mixed-metal complexes, on the other hand, show bands that do not correspond to either the pure $K[Ag(CN)_2]$ or pure $K[Au(CN)_2]$ starting material but to a metal−metal transition involving Ag and Au. The two emission bands due to Ag−Au interactions are observed at 343 and 372 nm. The intensity of the lower energy emission (372 nm) is affected by variations in the Au/Ag ratio and increases as the stoichiometric amount of Ag decreases, while the relative intensity of the higher energy emission band at 343 nm remains largely unaffected.

Figure 3 shows the three-dimensional emission spectra of the mixed-metal system $K[Au_{0.61}Ag_{0.39}(CN)_2]$ at 4.2 and 77 K. As the excitation wavelength is varied from 230 to 310 nm, different emission bands appear at different emission wavelengths, indicating the presence of different mixed-metal clusters of $Au(CN)_2^-$ and $Ag(CN)_2^-$. Since the $K[Ag(CN)_2]$ emission is at a higher wavelength than the $K[Au(CN)_2]$ emission, it follows that the higher energy peaks should have a greater amount of Ag than Au.

Comparison of the 77 K spectra with the 4.2 K spectra shows differences. The 77 K spectra show a decrease in intensity of the high-energy peaks observed at 4.2 K and an increase in the low-energy peaks seen at 4.2 K. This change in the relative intensity of the high-energy and low-energy peaks is due to energy transfer at 78 K between high-energy clusters and low-energy clusters. At 4.2 K, the barrier to energy transfer is larger than kT and energy transfer occurs very little. The results herein are similar to those we have reported for metal dicyanides such as $K[Au(CN)_2]$ and $K[Ag(CN)_2]$, both pure and doped, as impurities in KCl.[63,64]

In Figure 4, variable-temperature emission spectra are shown for $K[Au_{0.61}Ag_{0.39}(CN)_2]$ with $\lambda_{ex} = 265$ nm. We have previously published[44] a study of $K[Au(CN)_2]$ in which the

(63) Rawashdeh-Omary, M. A.; Omary, M. A.; Shankle, G. E.; Patterson, H. H. *J. Phys. Chem. B* **2000**, *104*, 6143−6151.
(64) Omary, M. A.; Hall, D. R.; Shankle, G. E.; Siemiarczuk, A.; Patterson, H. H. *J. Phys. Chem. B* **1999**, *103*, 3845−3853.

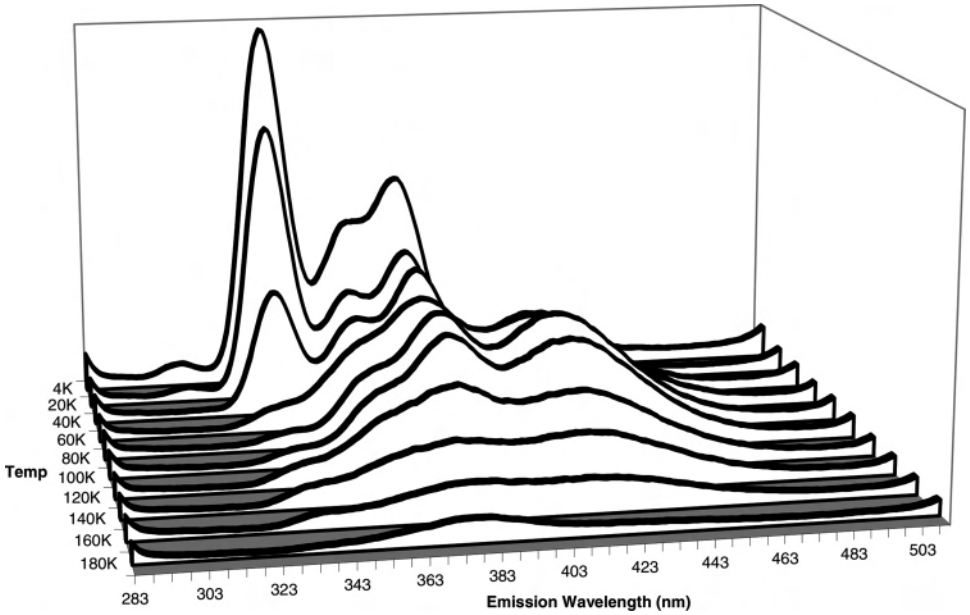

Figure 4. Variable-temperature emission spectra for the $K[Au_{0.61}Ag_{0.39}(CN)_2]$ crystal with $\lambda_{ex} = 265$ nm showing the intensity changes associated with the increase in temperature for each emissive species present in the crystal.

Table 3. Lifetime Data for Pure $K[Au(CN)_2]$ and $K[Ag(CN)_2]$ and Different Emission Bands Observed in $K[Au_{0.44}Ag_{0.56}(CN)_2]$ at 4.2 and 77 K

emission band, nm	lifetime at 4 K, μs	lifetime at 77 K, μs
415 ($K[Au(CN)_2]$)	12.90 ± 0.01	0.34 ± 0.01
390 ($K[Ag(CN)_2]$)	47.16 ± 0.02	44.63 ± 0.03
343 (Au−Ag mixed system)	0.076 ± 0.001	2.20 ± 0.02
372 (Au−Ag mixed system)	1.38 ± 0.02	2.27 ± 0.01

luminescence energy of the 390 nm peak and the unit cell dimension were recorded between 300 and 78 K. The emission energy showed a red-shift of 1100 cm^{-1} with a lowering of temperature and a decrease of intralayer Au−Au separation from 3.64 Å at 278 K to 3.58 Å at 78 K.[44] Thus, in mixed-metal crystals, we expect to observe a small red-shift of the emission peaks with lower temperature. However, in our previous studies of doped $Ag(CN)_2^-$ in KCl and NaCl, thermochromic behavior is observed[63] in which low-energy bands assigned to different clusters appear at higher temperature and higher energy clusters emission appear at low temperatures. The mixed-metal system reported herein has similar thermochromic behavior.

Lifetime measurements for the observed luminescence bands present in a d^{10} mixed-metal sample were carried out at 4.2 and 77 K. The results are summarized in Table 3. At 4 K, the 343 nm emission band shows a nanosecond lifetime, indicating that this process results from a singlet state (fluorescence) while the emission at 372 nm is significantly longer (1−3 μs), indicative of a phosphorescence process. Both pure $KAg(CN)_2$ and $KAu(CN)_2$ show microsecond scale lifetimes at 77 and 4 K, indicating this emission results from a phosphorescence process.

The luminescence lifetime for these species can be calculated using the equation $\tau = 1/(k_{rad} + k_{nonrad} + k_{mixed})$, where τ = lifetime, k_{rad} = rate constant of radiative energy transfer pathway, k_{nonrad} = rate constant of nonradiative energy transfer pathway, and k_{mixed} = rate constant for energy transfer within the mixed-metal cluster. The shorter lifetime values observed in the mixed-metal systems relative to the pure metal systems are indicative of the mixed metal systems (k_{mixed}) contribution to the lifetime. It should also be noted that the lifetime values at 4 K are smaller than those measured at 77 K. This is because, at higher temperatures, k_{mixed} decreases as a result of a decrease in the mixed metal delocalization. Thus, as a result, the value of τ increases with increasing temperature.

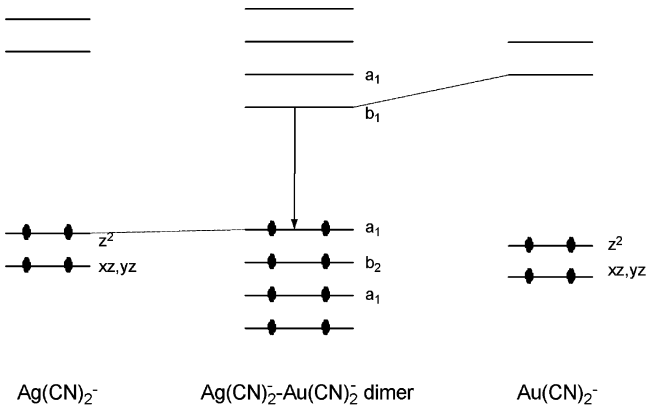

Figure 5. Energy level diagram for $[Au(CN)_2]^-$ ($D_{\infty h}$), $[Ag(CN)_2]^-$ ($D_{\infty h}$), and the mixed-metal $\{[Au(CN)_2^-]-[Ag(CN)_2^-]\}$ (C_{2v}) dimer showing the possible mixed-metal transition for the dimeric unit. The arrow represents the transition from an orbital that is mostly Au in character to an orbital that is mostly Ag in character.

Electronic Structure Calculations. Figure 5 shows the simplified energy level diagram obtained from relativistic extended Hückel calculations performed on the mixed-metal $[Au(CN)_2^-]-[Ag(CN)_2^-]$ dimer. The $[Au(CN)_2^-]$ and $[Ag(CN)_2^-]$ monomer units are both linear; the two subunits are eclipsed, and the Au−Ag bond lies along the *z* axis. The potential energy diagram (Figure 6) of the ground state of the $[Au(CN)_2^-]-[Ag(CN)_2^-]$ dimer shows a minimum at a Au−Ag separation of 3.45 Å. At this separation, the contribution to the HOMO of the Ag 5s, $d_{x^2-y^2}$, and d_{z^2} is

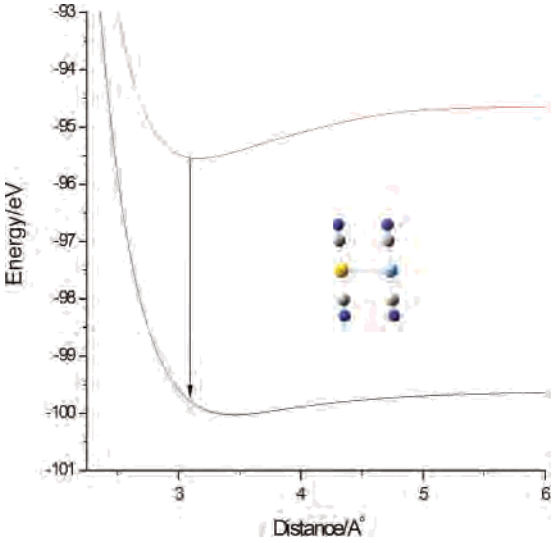

Figure 6. Potential energy diagram of the mixed-metal $[Au(CN)_2^-]-[Ag(CN)_2^-]$ dimer showing the first excited-to-ground-state transition. The excited state has a shorter metal−metal distance and a deeper potential well than the ground state, indicative of a stronger bonding relative to the ground state.

Table 4. Summary of Extended Hückel Calculations for the Pure and Mixed-Metal Dimers

system	M−M, eq	energy, eV	M−M*, eq	energy, eV	HOMO−LUMO, eV
$[Au(CN)_2^-]_2$	3.30	−102.385	3.00	−98.091	4.40
$[Au(CN)_2^-]-[Ag(CN)_2^-]$	3.50	−100.025	3.20	−95.546	4.61
$[Ag(CN)_2^-]_2$	3.70	−97.662	3.30	−92.928	4.91

slightly larger than the corresponding contribution from the Au. In the LUMO, however, the gold $5p_z$ orbital has a larger contribution than the $4p_z$ orbital of silver. The HOMO of the mixed-metal dimer can be characterized as having σ^* character, while that of the LUMO has π character. Previously published results for pure $[Ag(CN)_2^-]_2$ dimers indicate an antibonding HOMO,[64,65] while the LUMO is slightly bonding. This explains the shortening of the Ag−Au separation when an electron is promoted from the HOMO to the LUMO. Table 4 shows the summary of the extended Hückel calculations for the pure and mixed-metal dimers. As can be seen from this table, the HOMO−LUMO energy gap for the mixed-metal dimer lies in between the HOMO−LUMO energy gap for the pure gold and silver metal cases. This is consistent with the observation of a mixed-metal transition in the mixed-metal system.

In order to approximate the local environment of a linear $M(CN)_2^-$ ion (M = Ag, Au) in the crystal, extended Hückel calculations were performed on a series of systems where each $Au(CN)_2^-$ or $Ag(CN)_2^-$ is surrounded by four $M(CN)_2^-$ in a rectangular arrangement and a point group of D_{2h}. When the HOMO−LUMO gap was calculated at the equilibrium distance for each mixed-metal case, it was found that the energy of the mixed-metal clusters $([Au(CN)_2^-]_n-[Ag(CN)_2^-]_{n-1}$, $n = 1\rightarrow4)$ lies in between that of the pure $[Ag(CN)_2^-]_5$ and $[Au(CN)_2^-]_5$ cases. Surprisingly, values of

(65) Omary, M. A.; Patterson, H. H. *J. Am. Chem. Soc.* **1998**, *120*, 7696−7705.

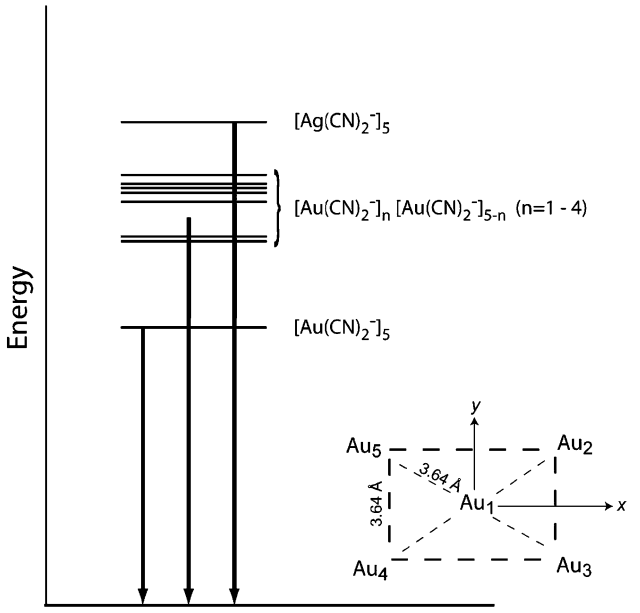

Figure 7. HOMO−LUMO energy gap for $[Au(CN)_2^-]_5$ (D_{2h}), $[Ag(CN)_2^-]_5$ (D_{2h}), and mixed-metal pentameric species. The crystallographic results indicate that every Au or Ag atom in a given layer has four nearest neighbors in a rectangular arrangement. The inset shows this rectangular arrangement of the Au atoms for the pentameric $[Au(CN)_2^-]_5$ species. Arrows represent the Ag and Au pure metal transitions, as well as the mixed-metal transition, all observed in the luminescence spectra shown in Figure 2.

Table 5. HOMO−LUMO Energy Gap from Extended Hückel Calculations for the Pure and Mixed-Metal $[Au(CN)_2^-]_n[Ag(CN)_2^-]_{n-1}$ ($n = 1\rightarrow4$) Units[a]

	HOMO−LUMO gap/cm^{-1}	HOMO−LUMO gap/nm
$[Ag(CN)_2^-]_5$	34019.5	294
$[Au(CN)_2^-][Ag(CN)_2^-]_4$	32862.2	304
$[Au(CN)_2^-]_2[Ag(CN)_2^-]_3$[b]	32681.0	306
$[Au(CN)_2^-]_2[Ag(CN)_2^-]_3$[c]	32511.5	308
$[Au(CN)_2^-]_4[Ag(CN)_2^-]$	32025.7	312
$[Au(CN)_2^-]_3[Ag(CN)_2^-]_2$	31602.9	316
$[Au(CN)_2^-]_5$	30838.4	324

[a] For the mixed-metal cases, one unit of $[Ag(CN)_2^-]$ is surrounded by four $[M(CN)_2^-]$ in a rectangular arrangement. [b] Linear arrangement of Ag atoms. [c] Bent arrangement of Ag atoms.

the HOMO−LUMO gap for the mixed-metal cases fall within an ~1000 cm^{-1} range. The result is summarized in Figure 7 and Table 5.

The results from the extended Hückel calculations for the pure and mixed-metal species indicate that exciting the different species with the appropriate wavelength will produce stable excimers supported by metal−metal interactions. The observed luminescence in the different mixed-metal systems are assigned to mixed-metal transitions, i.e., a transition from the lowest excited state with mostly Au in character to an orbital in the ground state that has mostly Ag character. The excitation spectrum at 4.2 K spans a broad range below 300 nm, indicating that there are a number of excited states leading to the emission of mixed-metal species with $\lambda_{em} < 400$ nm (see Supporting Information).

Emission bands at 343 and 372 nm in the Au−Ag mixed-metal systems reported herein have been assigned to mixed-metal transitions from extended Hückel calculations. These calculations suggest a stronger bonding interaction in the

lowest excited state but only a weak interaction in the ground state, as has been observed in other Au and Ag complexes. It should be noted that the magnitude of the distances and energies summarized in Table 4 from extended Hückel calculations are presented in a qualitative manner, and therefore, conclusions should not be drawn from the absolute values of these numbers. This is due to the low level of the calculations performed and the fact that the species are assumed to be in idealized geometry. However, qualitative comparisons between the different species can be made.

Conclusions

Crystals of the mixed-metal $d^{10}-d^{10}K[Au_xAg_{1-x}(CN)_2]$ heterometallic samples with different Ag/Au ratios have been synthesized and characterized. X-ray diffraction studies showed that the structure of the different mixed-metal systems are similar to each other and exhibits the similar layered structure found in pure $K[Au(CN)_2]$ and $K[Ag(CN)_2]$. The structure of $K[Au_{0.44}Ag_{0.56}(CN)_2]$ is isostructural to $K[Au(CN)_2]$, while $K[Ag(CN)_2]$ crystallizes in a different space group.

The emission bands observed in the mixed-metal complexes lie between the emission bands of the pure $K[Au(CN)_2]$ and $K[Ag(CN)_2]$. Variable-temperature luminescence studies showed that the emission maxima observed in the different $K[Au_xAg_{1-x}(CN)_2]$ ($x = 0 \rightarrow 1$) heterometallic samples do not change in energy as the Au/Ag ratio is varied and the cation has a +1 charge. This is in contrast with the previously reported $La[Au_xAg_{1-x}(CN)_2]_3$ ($x = 0 \rightarrow 1$) where the emission maxima are tunable with respect to the Au/Ag ratio and the counterion is +3.

Lifetime measurements were obtained for single crystals of $K[Au_xAg_{1-x}(CN)_2]$ at 77 and 4 K. At 4 K, the 343 nm emission band shows a nanosecond lifetime, indicating that this process results from a singlet state (fluorescence) while the emission at 372 nm is significantly longer ($1-3\ \mu s$), indicative of a phosphorescence process. Both pure $K[Ag(CN)_2]$ and $K[Au(CN)_2]$ show microsecond scale lifetimes at 77 and 4 K, indicating their observed emission results from a phosphorescence process. The increase in lifetime from 4 to 77 K for the emission at 372 nm is indicative of a decrease in the mixed-metal delocalization as temperature is increased.

Extended Hückel calculations revealed that the first excited states of the different trimeric species have shorter metal−metal separation, deeper potential energy wells, and stronger metal−metal interactions than the ground state. This is reflective of exciplex behavior. Further, in the mixed-metal systems, the observed luminescence has been assigned to a mixed-metal transition in which an electron jumps from the lowest excited state with mostly Au character to the ground state with mostly Ag character.

Acknowledgment. This work was supported by the National Science Foundation (CHE-0315877). We thank Mr. David LaBrecque for his assistance.

Note Added after ASAP Publication. This article was released ASAP on July 28, 2007 with minor errors in Tables 1 and 2. The correct version was posted on July 31, 2007.

Supporting Information Available: Crystallographic information files (CIF) and excitation spectra of the different pure and mixed-metal complexes. This material is available free of charge via the Internet at http://pubs.acs.org.

IC700780K